Percolation Models of Adsorption-Desorption Kinetics with Hysteresis

M. ŠOÓŠ and P. RAJNIAK*

Department of Chemical and Biochemical Engineering, Faculty of Chemical and Food Technology, Slovak University of Technology, SK-812 37 Bratislava
e-mail: soos@tech.chem.ethz.ch; pavol_rajniak@merck.com

Received 2 August 2001

The problem of kinetics for adsorption/desorption of condensable vapours in porous media is studied theoretically and experimentally. A finite two-dimensional (2D) lattice model with random size distributions of spherical pore sites and cylindrical pore connections fitted to experimental equilibrium data was further improved. Mathematical models of surface diffusion and condensation/evaporation in the lattice were developed and studied theoretically during adsorption/desorption. The theoretical models correctly predict qualitative and quantitative features of the experiments for the system Vycor glass—nitrogen.

The problem of predicting mass transfer rates of adsorbable vapours in porous media in the range of pressure where capillary condensation occurs is a significant one for the design and operation of adsorbers, dryers, catalytic reactors, *etc.* Like in adsorption-desorption equilibria, hysteresis has also been reported for the kinetics in the capillary condensation region. The concentration dependence of diffusivity exhibits a maximum during adsorption and a minimum during desorption. Various experimental methods used to determine the mass transport rates in the capillary condensation regime [1—4] and theoretical approaches explaining the experimental results [5—8] have appeared in the literature. Literature reports on hysteresis in the kinetics of adsorption/desorption include the study of capillary condensation flow of toluene in Vycor glass [1], gravimetric measurements of the kinetics of isothermal adsorption and desorption of isopropanol in Vycor glass [9], multilayer diffusion and capillary condensation of propylene in supported alumina films [10], permeabilities in Vycor glass [11], and isothermal transport of liquids in partially saturated packed beds of glass spheres [12]. Theoretical models used in these studies represent the classic continuous approach [13] and the complexities caused by the network effects were not considered.

In our recent works [14, 15] network models were formulated for predicting effective Fickian diffusivities of condensable vapours in porous media where capillary condensation and adsorption-desorption hysteresis occur. The models combine the equilibrium theory based on the pore-blocking interpretation of hysteresis in the interconnected network of pores [16—18] and the percolation model of mass transport in the network with randomly interspersed regions [19] for capillary condensation and surface flow. A new predictive model based on properties of Bethe lattices was proposed to account for the existence of liquid-filled "blind" pores that results in a maximum and subsequent decrease in the total diffusion rate. For desorption, a new "shell and core" representation of the network model was proposed. Information from adsorption-desorption equilibria was needed to compute the thickness of the shell in which desorption/evaporation occurs for concentrations higher than the percolation threshold.

However, there are several questionable assumptions in the analytical models presented in our previous contribution [15], the distinct boundary between the shell and the core, the use of effective medium approximation (EMA), and the use of Bethe tree for mass transfer during desorption.

This paper overcomes these disadvantages by using theoretical percolation models of diffusion and condensation/evaporation in the square lattice structure during adsorption/desorption. Comparison of numerical solutions with experimental kinetic data is also discussed.

EXPERIMENTAL

Commercial Vycor glass (Corning Inc.) was used as adsorbent in experiments. Vycor is a porous glass, which has been widely used as a model material in

*The author to whom the correspondence should be addressed.

studies of properties of fluids and molecules in highly confined geometries [20]. Kinetic data for nitrogen on Vycor glass at liquid nitrogen temperature 77 K were obtained using an Erba Sorptomatic 1900 apparatus, which is a fully automatic instrument for measuring the adsorption and desorption of gases (usually nitrogen) on a solid sample. A complete adsorption-desorption isotherm, which usually takes hours of operation, is obtained automatically. There was no influence by external diffusion, because pure nitrogen was used in the experiments.

In all diffusivity measurements, the sample initially at equilibrium was subject to a sudden small change in partial pressure of adsorptive and the changes of amount adsorbed during adsorption or desorption were continually recorded. The heat effects during the sorption measurements were minimized by allowing only small step changes in relative pressure during each measurement. Because the sorption rates were independent of the pellet size, we can assume that the total sorption rate was controlled by the mass transport processes within microparticles. Successive adsorption and desorption were conducted by changing the composition of the adsorptive and allowing adequate time to establish equilibrium [15].

THEORETICAL

We consider the adsorption-desorption process of a condensable vapour in a porous adsorbent. In Fig. 1*a* the adsorption-desorption equilibria for the process are shown. At relative pressure below point L, the lower closure point of the hysteresis loop, only surface adsorption occurs. Mass transport rates in this region are the same for both adsorption and desorption. Above point U, the upper closure point of the hysteresis loop, all pores become filled with capillary condensate. Transport of liquid condensate in the region above point U occurs by hydraulic pressure. The study of the kinetics in this region is out of scope of this work. In this contribution we are mainly interested in the mass transport rate in the region of simultaneous surface diffusion and capillary condensation, *i.e.* in the region between points L and U.

Kinetics of Adsorption

Mass transport in the capillary condensation region is a complex phenomenon. The conditions under which capillary condensation occurs are also those under which significant surface diffusion is expected. Vapour phase transport is in this case usually orders of magnitude smaller than the surface flow because of the relatively small amount of molecules in the vapour phase compared to that in the adsorbed phase [1, 9]. It is now generally recognized that the capillary suction accompanying condensation is a significant accelerator of the mass transfer [1, 11, 14, 15, 21]. Any capillary condensate volume elements create a short-circuit effect leading to a reduction in the length of the diffusion path and a corresponding increase in the effective diffusivity. So, the first effect of the capillary condensation is to increase the mass transport rate when some pores are filled with condensate. However, in real porous adsorbents, there exist blind (dead-end) pores. These blind pores are accessible for filling by surface adsorption and capillary condensation; but after filling with capillary condensate, they do not increase the total mass transport rate, but on the contrary, decrease it, because they do not conduct the flow. The fraction of pores that belongs to blind clusters will increase with increasing pressure. Therefore, in real porous adsorbents with the presence of the blind pores, all three main mechanisms (surface diffusion, capillary condensation, and liquid flow of capillary condensate) may already be operative simultaneously below point U. Subsequently a maximum in the total mass transfer rate exists during adsorption at a relative pressure $x < x^{\mathrm{U}}$, as shown in Fig. 1*b*.

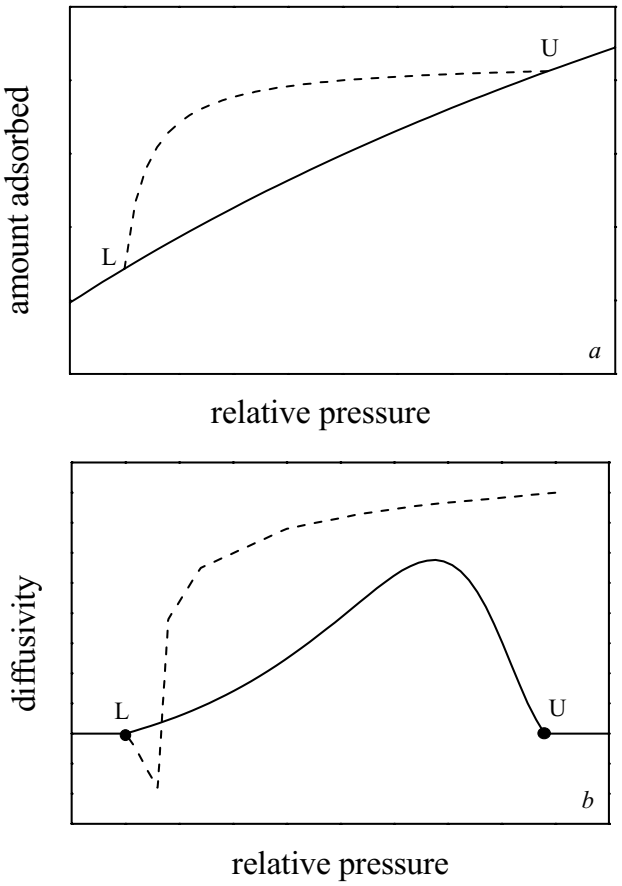

Fig. 1. Experimental hysteresis-dependent adsorption-desorption equilibria and kinetics. *a*) Equilibria; L = lower limiting point, U = upper limiting point of the hysteresis loop; *b*) kinetics: adsorption (——); desorption (– – –).

Kinetics of Desorption

Physical situation is different for the case of desorption or evaporation of the condensed adsorbate. While the condensation generally increases the mass transport rate, evaporation is a slow process and one can expect a decrease in the total mass transport rate with an increasing role of evaporation from pores. At high relative pressure $x < x^{\mathrm{U}}$ desorption occurs only from widest pores at the external surface of the finite microparticles of adsorbent. Large pores in the core of the microparticle cannot empty in this step, because they are blocked by smaller neighbouring pores and narrow pore connections. Total mass transport rate is relatively high, because the length of mass transport path is short. The boundary of the phase separation penetrates along the widest pores and connections into the microparticle volume. In this step the mass transport path increases and desorption rate decreases with decreasing pressure. At the relative pressure x^{T} corresponding to percolation threshold for desorption, there is a sufficient number of pore connections in which adsorbate is below its condensation pressure (and thus it is present as either metastable liquid or vapour) and desorption from the bulk of adsorbent starts. Mass transport path is complicated and long and desorption rate is very slow. Next decrease of pressure causes that higher and higher number of vapour-filled pore connections exists and total mass transport rate again increases. Subsequently a minimum in the total mass transfer rate exists during desorption at a relative pressure $x^{\mathrm{L}} < x < x^{\mathrm{U}}$, as shown in Fig. 1*b*.

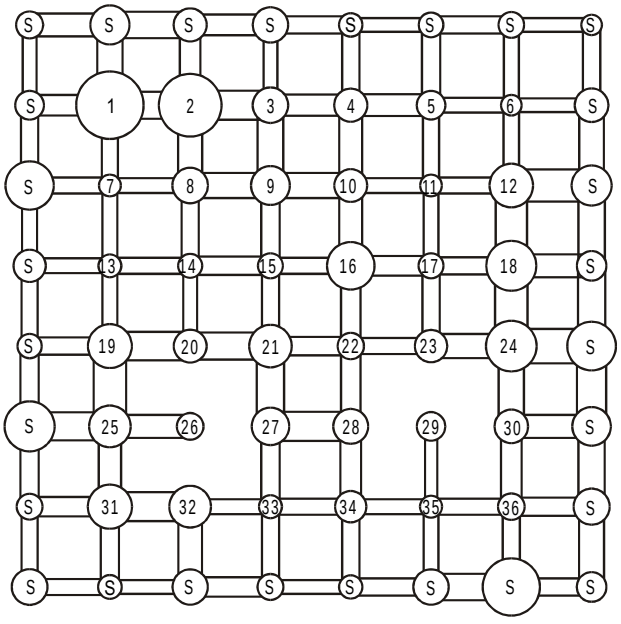

Fig. 2. Square (2D) lattice of spherical pore sites and cylindrical pore connections as a model of porous adsorbent. S = surface pores; 26, 29 = blind pores.

Square Lattice Model of Porous Adsorbent

Theoretical part of this work was carried out by the method of numerical simulations of adsorption and desorption on square lattice (2D) models of different dimensions [22]. Small version (8×8) of the lattice is shown in Fig. 2. The spherical pore cavities (sites, voids) are connected to each other by cylindrical connections (necks, throats). There are also "blind" pores in the lattice, which are accessible for filling by surface adsorption and capillary condensation; but after filling with capillary condensation, they do not conduct the flow.

The pore sites are placed at the nodes and the connections along the bonds of the lattice. The pore sites volume is calculated following its characteristic radius and it is assumed that the pore volume resides entirely in the pore sites. Negligible volume of each connection was supposed. The generation of the pore sites for any experimental adsorption-desorption systems is simpler and is associated with the experimental primary adsorption isotherm. On the other hand, the generation of the pore connections is more complicated and is associated with the primary desorption branch of the main hysteresis loop. In Fig. 3*a* the experimental equilibrium data for the system Vycor glass—nitrogen are shown. Corresponding size distribution functions for pore sites and pore connections are presented in Fig. 3*b*.

In our previous work [22], various explicit distribution functions were tested and used for pore cavities and pore connections. In this work the size distribution function of spherical pore cavities was evaluated from adsorption isotherm shown in Fig. 3*a* using the method of *Broekhoff* and *De Boer* [23]. The size distribution function of cylindrical pore connections was evaluated from desorption isotherm of Fig. 3*a* by an iterative procedure. The procedure was based on the assumption that radii of all connections of a cavity are smaller than the cavity radius. An arbitrary sharp distribution function for connections, which overlaps the cavity size distribution function, was used as initial approximation. However, the initial function was iteratively improved by fitting to desorption experimental data employing percolation theory for primary desorption [15]. Evaluated distribution functions (number basis) are presented in Fig. 3*b* for 23×23 square lattice. Next, the porous structure was reconstructed in the form of 2D square lattice composed of spherical pore cavities and cylindrical pore connections (Fig. 2). Significant improvement of primary adsorption isotherm was obtained compared to our previous work [22]. A better agreement between experimental and computed desorption equilibrium curve can be expected for $C > 4$, which is allowed only for other (*e.g.* cubic 3D or triangular 2D) lattices. Non-ideal square lattices in which some connections are missing may contain also blind (dead-end) pores, as

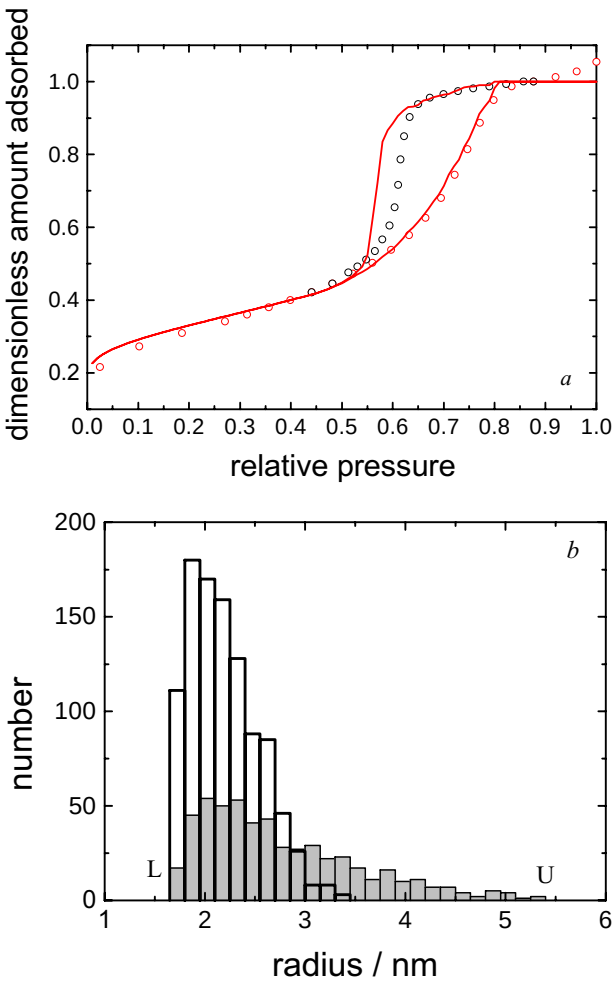

Fig. 3. *a*) Experimental (○) and computed (——) hysteresis-dependent adsorption-desorption equilibria for the systems Vycor glass—nitrogen with 23 × 23 square lattice. *b*) Corresponding histograms of distribution functions (number basis) fitted to the experimental data. □ Pore sites; ■ pore connections.

discussed above and shown in Fig. 2. More details about the fitting procedure and about generation of different lattices are given in our recent work [22]. The lattices obtained by fitting to equilibrium data were regenerated and used for modelling of mass transfer during adsorption and desorption.

Modelling of Mass Transport in Square Lattice

Additional assumptions for the mass transport modelling in the square lattice are:

1. Parameter φ (diffusivity multiplied by cross-section area divided by length) is a basic mass transfer coefficient in each connection for lattice with connections of constant lengths and constant cross-sections. Relative value of conductance d_{ji} of a connection ji between sites i and j is given only by the transport mechanism (surface diffusion, capillary condensation) in the connection and is independent of the connection radius R_{ji} and length L_{ji}.

2. ΔV_i is volume of pore site to be filled or to be emptied during each adsorption or desorption step, and is calculated for the difference Δx between starting and final relative pressure of the step.

3. Adsorbate concentration $c_i(\tau)$ in the i-th pore site (as well as concentrations $c_j(\tau)$ in the neighbouring sites j) is defined as fraction of ΔV_i, which is filled at time τ.

4. The thickness of adsorption film, t, in the pores and connections for pressures lower than the critical pressure from the Kelvin equation is computed from the empirical relation

$$\{t\} = 0.354 \left[\frac{-5}{\ln(x)}\right]^{1/3} \qquad (1)$$

5. Condensation in the cylindrical pore connection with radius R_{ji} starts if

$$\{R_{ji} - t\} < \frac{4.7}{\ln(1/x)} \qquad (2)$$

6. Condensation in the spherical pore site with radius R_i starts if

$$\{R_i - t\} < \frac{9.4}{\ln(1/x)} \qquad (3)$$

Eqns (*2*, *3*) are alternative forms of the Kelvin equation valid for condensation of nitrogen at 77 K [24].

7. Adsorbate concentration in the pore sites at the edges of the lattice (surface sites) is always in equilibrium with the relative pressure at the lattice surface.

8. Total amount adsorbed in the lattice can be computed by summation of all pore volumes filled by surface adsorption or capillary condensation. In other words, the densities of adsorption film and condensate are equal.

9. An "effective Fickian diffusivity" in the lattice can be evaluated by fitting the computed uptake curve to the solution of the diffusion equation (Fick's law).

Then the mathematical model of mass transport in 2D square lattice presented in Fig. 2 contains

– transient mass balances for internal pore sites

$$\Delta V_i \frac{\mathrm{d}c_i(\tau)}{\mathrm{d}\tau} = \sum_j \varphi\, d_{ji}\,[c_j(\tau) - c_i(\tau)] \quad i = 1, \mathrm{NI} \qquad (4)$$

– boundary conditions (adsorbate concentrations in surface pores) for adsorption

$$c_s = 1 \quad s = 1, \mathrm{NS} \qquad (5a)$$

– boundary conditions for desorption

$$c_s = 0 \quad s = 1, \mathrm{NS} \qquad (5b)$$

Thickness of adsorbed phase, t, was used as dependent variable in balance eqns (*4*) after simple transformation. The system of differential equations was solved using semi-implicit Runge—Kutta method (STIFF3 subroutine in [25]) in combination with effective LU factorization and solution of linear equations with sparse band coefficient matrix (subroutines LFTRB and LFSRB from IMSL library). Simulations for different adsorption steps were performed similarly as real experiments, *i.e.* for an increment Δx of relative pressure around the lattice surface the mass balances were integrated until reaching equilibrium in all sites. During the integration the Kelvin equation for connections (eqn (*2*)) and for pore sites (eqn (*3*)) was permanently tested. After reaching the condensation pressure in any connection *ij*, the relative diffusivity d_{ji} was increased to arrange acceleration of the mass transport process *via* suction. Subsequently, after reaching the Kelvin pressure in the i-th site, the diffusivities d_{ji} of all connections of the i-th site were again increased to realize further amplification of the mass transfer process. The adsorption algorithm for lattices with blind pores (for $C < 4$) was more complicated, because the existence and growth of blind clusters were tested during simulations. Diffusivities $d_{ji} = 0$ for connections between blind pores were employed and the mass transport process was stopped in the pores. Desorption algorithm was further complicated by the pore blocking in the network. Whether a pore is emptying during the desorption step depends upon whether at least one of its connections is connected to the vapour, and can also allow a capillary meniscus to pass (eqn (*2*)). The same relative diffusivities of pore connections were employed for both, condensation and evaporation. Then the only factor reducing the total desorption rate was prolongation of the mass transport path by pore blocking. After evaporation of the liquid from the pore site, there still remains an adsorbed film in both, the pore site and in pore connections, corresponding to the value of relative pressure and next emptying occurs *via* surface diffusion.

RESULTS AND DISCUSSION

Kinetic properties of the system Vycor glass—nitrogen were studied. In all figures the experimental and theoretical diffusivities are normalized. The data are rationed against the diffusivity at the lower closure point D_0. First, we tested basic qualitative properties of the kinetic models. The impact of the lattice size on evaluated Fickian diffusivities is presented in Fig. 4*a*, *b*.

As observed experimentally [15], the concentration dependence of the normalized diffusivity exhibits a maximum for adsorption. The maximum value increases with the lattice size as manifestation of the increasing mass transport path for larger lattices. Standard deviations 4—12 % were evaluated from 10 simulations with randomly generated 20 × 20 lattices (Fig. 4*b*). Relative diffusivities employed in adsorption simulations were $d_{ji} = 1$ for surface diffusion, $d_{ji} = 2$ for condensation in the connection *ji*, and $d_{ji} = 5$ for condensation in the site i.

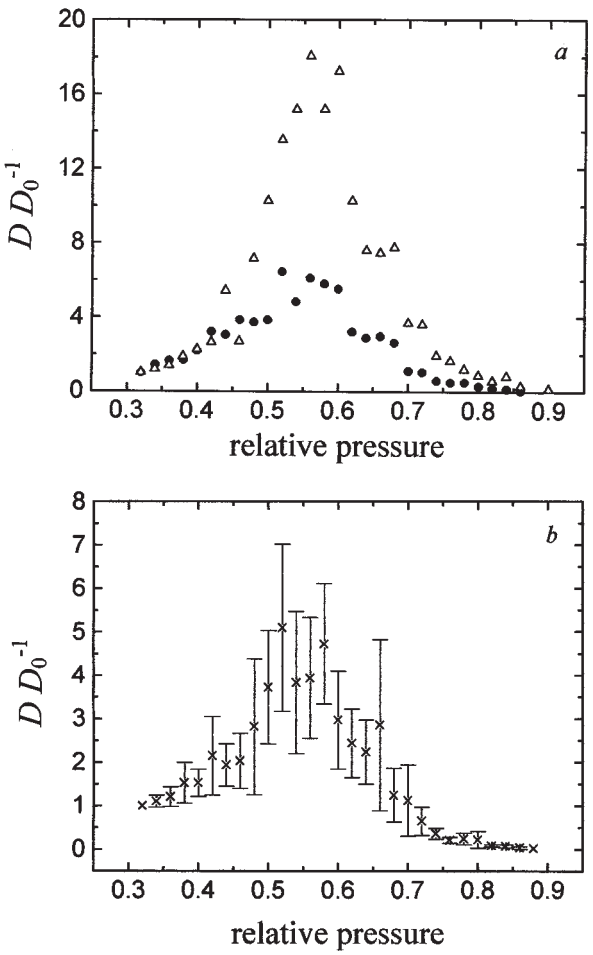

Fig. 4. Impact of lattice size on the computed effective diffusivity for adsorption. *a*) Lattice dimensions: 50 × 50 (△), 30 × 30 (●); *b*) lattice dimension 20 × 20, average values and error bars evaluated from 10 simulations.

Impact of the lattice size on desorption simulations is presented in Fig. 5*a*, *b*. The concentration dependence of the normalized diffusivity exhibits a minimum. Again, the difference between the minimum and maximum diffusivity increases with the lattice size. Standard deviations 6—22 % were evaluated from 10 simulations with randomly generated 20 × 20 lattices (Fig. 5*b*). Relative diffusivities employed in desorption simulations were $d_{ji} = 1$ for surface diffusion and $d_{ji} = 5$ for evaporation from any adjoining site i or j. This is a significant difference compared to our previous work [15] in which we assumed lower pore diffusivities for evaporation than for surface diffusion. The process of evaporation from an individual pore site, which is typically in metastable

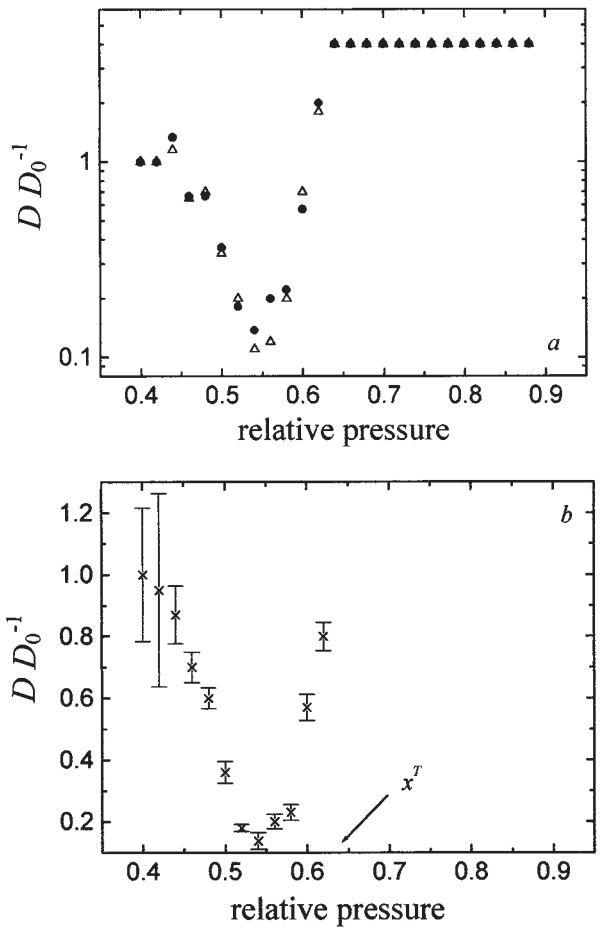

Fig. 5. Impact of lattice size on the computed effective diffusivity for desorption. *a*) Lattice dimensions: 30 × 30 (△), 20 × 20 (●); *b*) lattice dimension 20 × 20, average values and error bars evaluated from 10 simulations.

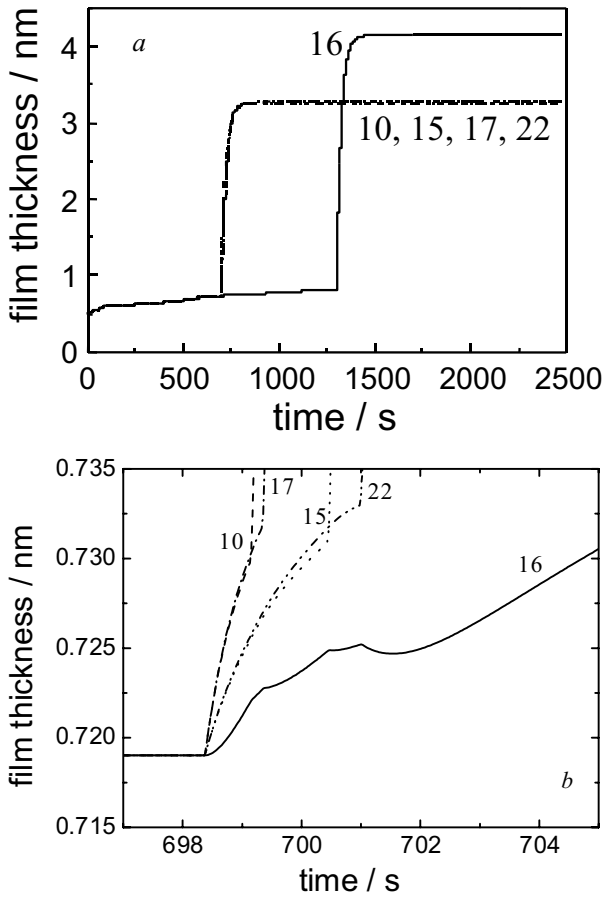

Fig. 6. Time dependence of adsorbed film thickness during adsorption inside the pores from Fig. 2. *a*) Complete transients for central pore 16 and its four neighbours; *b*) detailed inset for filling of the pores at the onset of capillary condensation.

state, can be very quick. Simulations confirm that the reason of the slow desorption close to percolation threshold is long and complicated mass transfer path in the lattice with many blocked connections and pores.

Next, some interesting features of the kinetic models are discussed. Time dependence of the adsorbed film thickness, t, during adsorption inside the pores is shown in Fig. 6. In Fig. 6*a* we can observe much slower filling by the surface diffusion compared to rapid and robust capillary condensation illustrated by practically vertical lines.

Because the capillary condensation commences almost simultaneously in all four neighbours of the pore 16, there exists a local minimum of the film thickness in the pore 16 as manifestation of the adsorbate suction by its neighbours, as illustrated in Fig. 6*b*.

Interesting behaviour can be observed also during desorption in the same subsystems of pores, as presented in Fig. 7.

Comparing Fig. 6*a* and Fig. 7*a* we can see that capillary condensation starts in the pore 10 and then subsequently in pores 17, 15, 22, and 16. On the other hand, the evaporation from the same pores occurs in the order: 10, 16, 15, 22, and 17 as a consequence of pore blocking in the network. Fig. 7*b* shows the existence of maxima on the time dependences of the film thickness for pores 10 and 4 when large amount of adsorptive evaporating from pore 16 passes through the pores to the lattice surface.

Experimental data of the normalized Fickian diffusivity for desorption for the system Vycor glass—nitrogen are shown in Fig. 8. Comparisons to the theoretical predictions by desorption model of this work, as well as by "shell and core" model [15], are presented in the figure. Both theoretical models are able to predict well, qualitatively, the experimental concentration dependence of the diffusivity. Less satisfactory prediction of the minimum position by the lattice model is a consequence of unsatisfactory prediction of the primary desorption curve by this 2D model, as already presented in Fig. 3. Compared to our previous work [15] the quantitative agreement was significantly improved, too.

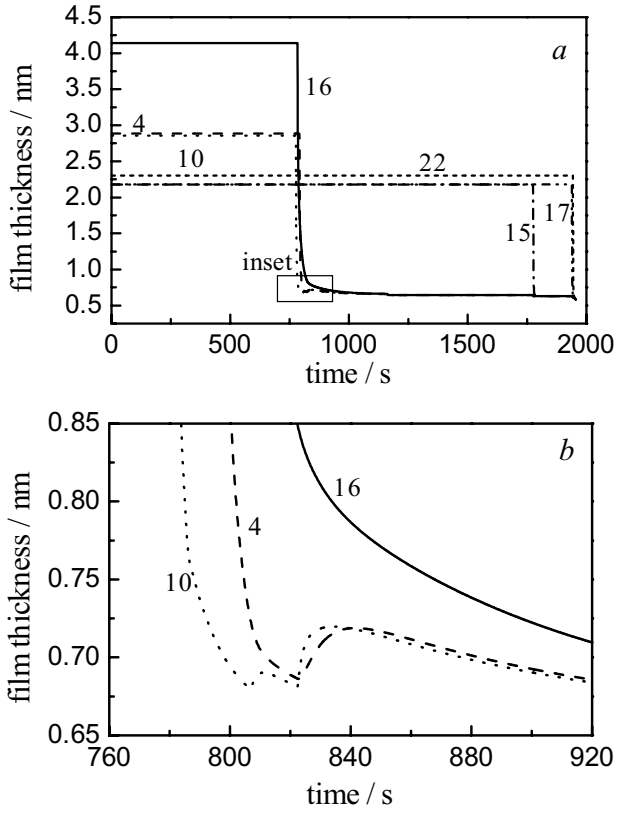

Fig. 7. Time dependence of adsorbed film thickness during desorption inside the pores from Fig. 2. *a*) Complete transients for central pore 16 and its four neighbours; *b*) detailed inset for emptying of the pores.

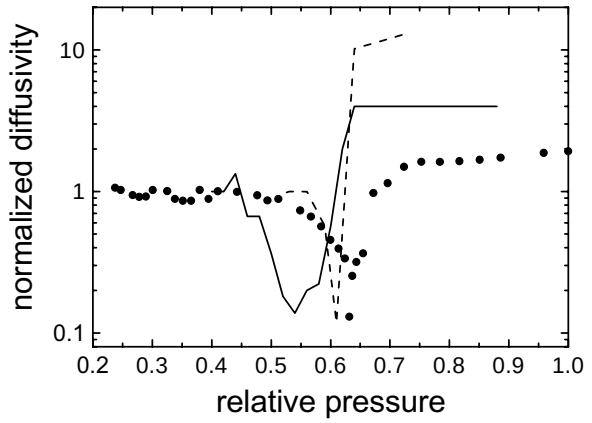

Fig. 8. Experimental diffusivity data (●) *vs.* theoretical predictions by using lattice model (——) and "shell and core" model (– –).

CONCLUSION

Percolation square lattice models are formulated for modelling of mass transport during adsorption and desorption of condensable vapours in porous adsorbent. Sorption kinetics is studied both experimentally and theoretically. The main results are as follows:

1. Kinetic models satisfactorily predict maximum of the Fickian diffusivity for adsorption as well as minimum for desorption.

2. Significant improvement of the quantitative agreement with experimental data for desorption was achieved assuming higher pore diffusivities for evaporation from pores. Simulations indicate that the prolongation of the mass transport path from the core of the sorbent microparticles is the main reason of the slow desorption close to the percolation threshold.

3. Unsatisfactory prediction of the primary desorption equilibrium by the simple 2D model influences the position of predicted minimum on the concentration dependence of normalized Fickian diffusivity. Both problems can be solved employing lattices (*e.g.* 2D triangular or 3D cubic) with connectivity $C > 4$.

4. Adsorption model predicts interesting theoretical transient behaviour in the selected pores with possible local minima of the adsorbed film thickness as a consequence of suction of adsorbate by neighbouring pores in which capillary condensation occurs.

5. Desorption model predicts local maxima of the film thickness as a consequence of evaporation of adsorbate from neighbouring pore.

6. Filling or emptying of the same pores can start in very different order, because of pore blocking during desorption.

7. Models proposed in this work represent next step in unification of the theories for equilibrium and kinetics for systems with hysteresis. Information on the adsorption-desorption equilibria are used for prediction of kinetic behaviour.

Acknowledgements. This project was financed by the Grant Agency of the Slovak Republic (Grant VEGA 1/7351/20).

SYMBOLS

C	connectivity	
$c_i(\tau)$	adsorbate concentration	
D	diffusivity of the whole network	$m^2\ s^{-1}$
D_0	diffusivity D at the lower closure point	$m^2\ s^{-1}$
d_{ji}	relative diffusivity for the connection between pore i and j	
φ	basic mass transport coefficient	$m^3\ s^{-1}$
L_{ji}	length of the cylindrical pore connection	m
L	lower limiting point	
N	number of pore sites in each row or column of the $N \times N$ lattice	
NI	number of internal pore sites of the lattice NI $= (N-2) \times (N-2)$	
NS	number of surface pore sites of the lattice NS $= 4 \times (N-1)$	
R_{ji}	radius of the cylindrical pore connection	nm
R_i	radius of the spherical pore site	nm
T	temperature	K
t	thickness of adsorbed film	nm

τ	time	s
U	upper limiting point	
ΔV	part of pore volume filled or emptied during a sorption step	m^3
x	relative pressure	
Δx	increment of relative pressure for a sorption step	

Subscripts

i, j	indices for pore connections and pore sites
s	surface

Superscripts

L	lower limiting point
U	upper limiting point
T	percolation threshold

REFERENCES

1. Abeles, B., Chen, L. F., Johnson, J. W., and Drake, J. M., *Isr. J. Chem. 31*, 99 (1991).
2. Rhim, H. and Hwang, S.-T., *J. Colloid Interface Sci. 52*, 174 (1974).
3. Tamon, H., Okazaki, M., and Toei, R., *AIChE J. 27*, 271 (1981).
4. Toei, R., Imakoma, H., Tamon, H., and Okazaki, M., *J. Chem. Eng. Jpn. 16*, 431 (1983).
5. Carman, P. C., *Proc. R. Soc. London 203*, 55 (1950).
6. Gilliland, E. R., Baddour, R. F., and Russell, J. L., *AIChE J. 4*, 90 (1958).
7. Kapoor, A. and Yang, R. T., *Chem. Eng. Sci. 44*, 1723 (1989).
8. Flood, E. A., Tomlinson, R. H., and Leger, A. E., *Can. J. Chem. 30*, 389 (1952).
9. Haynes, J. M. and Miller, R. J., in *Adsorption at the Gas-Solid and Liquid-Solid Interface.* (Rouquerol, J. and Sing, K. S. W., Editors.) P. 439. Elsevier, Amsterdam, 1982.
10. Uhlhorn, R. J. R., Keiser, K., and Burggraaf, A. J., *J. Membr. Sci. 66*, 259 (1992).
11. Lee, K.-H. and Hwang, S.-T., *J. Colloid Interface Sci. 110*, 544 (1986).
12. Bussing, W., Bart, H. J., and Germerdonk, R., *Int. J. Heat Mass Transfer 39*, 1925 (1996).
13. Sahimi, M., Gavalas, G. R., and Tsotsis, T. T., *Chem. Eng. Sci. 45*, 1443 (1991).
14. Rajniak, P. and Yang, R. T., *AIChE J. 42*, 319 (1996).
15. Rajniak, P., Šoóš, M., and Yang, R. T., *AIChE J. 45*, 735 (1999).
16. Rajniak, P. and Yang, R. T., *AIChE J. 39*, 774 (1993).
17. Rajniak, P. and Yang, R. T., *AIChE J. 40*, 913 (1994).
18. Mason, G., *Proc. R. Soc. London a Mat 415*, 453 (1988).
19. Burganos, V. N. and Sotirchos, S. V., *AIChE J. 33*, 1678 (1987).
20. Page, J. H., Liu, J., Abeles, B., Deckman, H. W., and Weitz, D. A., *Phys. Rev. Lett. 71*, 1216 (1993).
21. Weisz, P. B., *Phys. Chem. 79*, 798 (1975).
22. Šoóš, M. and Rajniak, P., *Chem. Pap. 55,* 391 (2001).
23. Broekhoff, J. C. P. and De Boer, J. H., *J. Catal. 10*, 153 (1968).
24. Gregg, S. J. and Sing, K. S. W., *Adsorption Surface Area and Porosity.* 2nd Edition. Academic Press, London, 1982.
25. Villadsen, J. and Michelsen, M. L., *Solution of Differential Equation Models by Polynomial Approximation.* Prentice Hall, Englewood Cliffs, New Jersey, 1978.